

Training Algorithm Matters for the Performance of Neural Network Potential: A Case Study of Adam and the Kalman Filter Optimizers

Yunqi Shao,¹ Florian M. Dietrich,¹ Carl Nettelblad,² and Chao Zhang¹

¹*Department of Chemistry-Ångström Laboratory, Uppsala University, Lägerhyddsvägen 1, BOX 538, 75121, Uppsala, Sweden*

²*Division of Scientific Computing, Department of Information Technology, Uppsala University, Lägerhyddsvägen 2, BOX 337, 75105, Uppsala, Sweden*

(*Electronic mail: chao.zhang@kemi.uu.se)

(Dated: 10 November 2021)

One hidden yet important issue for developing neural network potentials (NNPs) is the choice of training algorithm. Here we compare the performance of two popular training algorithms, the adaptive moment estimation algorithm (Adam) and the Extended Kalman Filter algorithm (EKF), using the Behler-Parrinello neural network (BPNN) and two publicly accessible datasets of liquid water [Proc. Natl. Acad. Sci. U.S.A. 2016, 113, 8368-8373 and Proc. Natl. Acad. Sci. U.S.A. 2019, 116, 1110-1115]. This is achieved by implementing EKF in TensorFlow. It is found that NNPs trained with EKF are more transferable and less sensitive to the value of the learning rate, as compared to Adam. In both cases, error metrics of the validation set do not always serve as a good indicator for the actual performance of NNPs. Instead, we show that their performance correlates well with a Fisher information based similarity measure.

I. INTRODUCTION

Neural network potentials (NNPs) are one category of machine learning potentials¹⁻⁴ which approximate potential energy surfaces (PES) and allow for large-scale simulations with the accuracy of reference electronic structure calculations but at only a fraction of the computational cost⁵.

One prominent architecture of NNPs are Behler-Parrinello neural networks⁶ which introduced the idea of partitioning the total potential energy of the system into effective atomic contributions. BPNNs have been applied to a wide range of molecules and materials⁷⁻¹² Despite these successes, the BPNN architecture relies on the selection of a set of symmetry functions before the training in order to describe the local chemical environments. On the contrary, features in deep-learning¹³ are automatically learned via hierarchical filters, rather than handcrafted. In particular, graph convolution neural networks (GCNN), which consider the atoms as nodes and the pairwise interactions as weighted edges in the graph, have emerged as a new type of architectures in constructing NNPs for both molecules and materials¹⁴⁻¹⁶.

Innovations regarding new architectures certainly drive the improvement of the performance of NNPs. However, one hidden and less discussed issue is the impact of training algorithms on the construction of NNPs. As a matter of fact, earlier implementations of BPNNs¹⁷⁻²¹ used either the Limited-memory Broyden-Fletcher-Goldfarb-Shanno algorithm (L-BFGS)²² or the Extended Kalman Filter algorithm (EKF)²³ as the default optimizer, while recent implementations of GCNN architectures^{14-16,24} almost exclusively chose the adaptive moment estimation algorithm (Adam)²⁵ instead. This contrast is, partly, due to the convenience that efficient implementations of Adam are available on popular frameworks such as TensorFlow²⁶ and Py-

Torch²⁷. Nevertheless, the practical equivalence among optimization algorithms for training NNPs is assumed rather than verified.

In principle, comparing training algorithms for the performance of NNPs is a highly non-trivial task. This largely comes from the fact that the final performance of NNPs is affected by many different factors which could convolute the comparison. These include the construction of dataset, the setup of loss function and batch schedule, the choice of neural network architecture, the hyperparameters of training algorithm, not to mention human errors in implementing these training algorithms and the corresponding neural network architecture. Even everything is properly controlled, the ground truth to judge the effect of training algorithm on the performance of NNPs in real-application scenarios may simply not be available.

To carry out this daunting task, our strategy is to use published datasets of liquid water where credible reference values in real-application scenarios are available^{8,9}. This allows us to just focus on the effect of training algorithm, while the rest of hyperparameters, i.e. the NNP architecture (setups of the BPNN and symmetry functions), the loss function and the batch schedule, in addition to the dataset, can be inherited and kept fixed. To minimize the impact due to differences in implementation, we implement EKF in the TensorFlow-based PiNN code¹⁶, where the BPNN architecture was previously implemented and tested. The technical soundness of our implementation of EKF is verified against the EKF implementation in the RuNNer code¹⁹, which was used to generate NNPs in the reference works with the same datasets^{8,9}. In this way, we can compare EKF and Adam on an equal footing, where the native implementation of Adam in Tensorflow is used.

Before showing these results, we will outline the details of our comparative study, including the training algo-

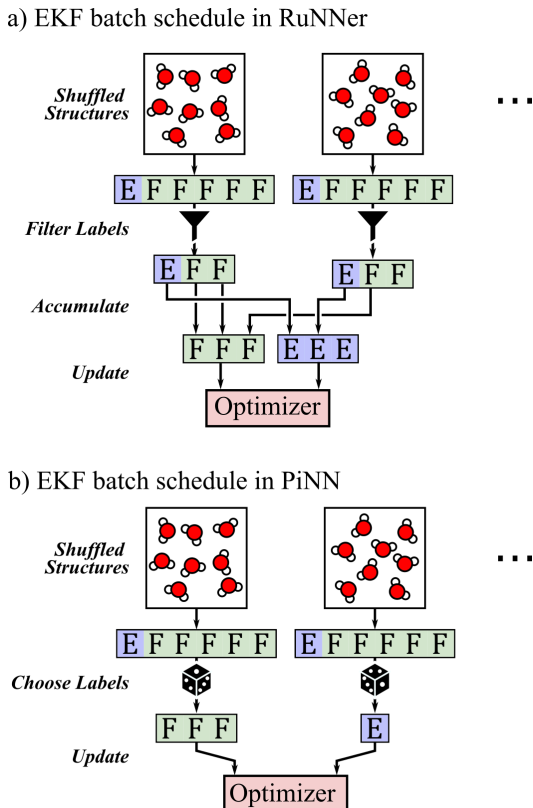


FIG. 1. Illustrations of the batch schedule of energy (E) and force (F) labels in a) RuNNer and b) PiNN. This is designed for EKF and used in Adam for the comparative study here.

rithms, datasets, the network architecture, and molecular dynamics simulations used for the density prediction, as described in the next section.

II. METHODS

A. Loss Function and Batch Schedule

As the aim in this study is to elucidate the effect of training algorithm on the performance of NNPs, the definition of loss function and the choice of batch schedule need to be held consistent between EKF and Adam algorithms.

We denote $\hat{\mathbf{y}}(\mathbf{w}, \mathbf{x})$ as the neural network prediction given the weight vector \mathbf{w} and input vector \mathbf{x} , and \mathbf{y} as the training-data labels. Here, we define $\boldsymbol{\xi} = \sqrt{c/n}(\hat{\mathbf{y}} - \mathbf{y})$ as the scaled error vector, where n is the size of vector \mathbf{y} and c is the weighting factor (for balancing number of energy and force labels). This leads to the L_1 loss function as $L_1 = \sum_i |\xi_i|$. The corresponding L_2 loss function $L_2 = \sum_i \xi_i^2$ is then related to the mean squared error scaled by c . Since EKF minimizes the error vector $\boldsymbol{\xi}$ and Adam minimizes the L_2 loss, this setup ensures that two algorithms optimize the same loss function as long as training data are the same.

Another distinction between the two algorithms (without diving into the details, as elaborated in the next Section) is on the batch schedule. EKF, as originated from the field of control theory and signal processing²⁸, is designed for on-line training (i.e. one training data-point at a time), in contrast to the mini-batch (a group of randomly selected training data) often used in Adam. This difference becomes blurred when the multi-stream variant of EKF is employed.²⁰ Nevertheless, we followed the practice of doing weight-update step based on either energy or force as in the previous studies, to avoid the complication of combining energy and force data in one step.²⁰

In the RuNNer setup of EKF, the weights are updated when a given number of error and corresponding Jacobian is computed. As the number of force labels overwhelms that of energy labels, a small fraction of force labels is typically used²⁰. In addition, the labels can be filtered according to the magnitude of the error, which potentially improves the efficiency. An illustration of the batch schedule used in RuNNer is shown in Fig. 1a.

Here, we choose to apply a simplified scheme of batch schedule in which the weight update is based on randomly selected force or energy label in each iteration without filtering, which is computationally more efficient in TensorFlow. In our particular instance, it is one energy label or ten force labels for each iteration, as illustrated in Fig. 1b. As shown in Result and Discussions, this simplification in batch schedule does not incur an inferior performance of the NNPs optimized with EKF. Subsequently, the same batch schedule is used in Adam for the sake of consistency.

Further details regarding the loss function and batch schedule, including the estimated number of weight updates based on energy and forces in each scheme and the weighting factor c thereof, are listed in the Supplementary Material (Section B).

B. Algorithms

In the following, we first introduce the common notations used for the optimization algorithm, and then briefly state the Adam and EKF algorithms compared within this work.

Continuing from the previous section, we denote \mathbf{g} as the gradient of the L_2 loss function with respect to the weight vector \mathbf{w} , and \mathbf{J} is the Jacobian matrix of $\boldsymbol{\xi}$ with respect to \mathbf{w} .

The first optimization algorithm used in this work is Adam, which is a popular algorithm for the training of neural networks.²⁵ The algorithm can be considered as an extension of stochastic gradient descent in which the first moment $\mathbf{m}(t)$ and second moment $\mathbf{v}(t)$ are estimated at each step, and used as a preconditioner to the gradients.

The algorithm is shown in Algo. 1.

Algorithm 1: The Adam optimizer, where η is the learning rate, ϵ is a small number, β_1, β_2 are the exponential moving average factors, \mathbf{m}, \mathbf{v} are the first and second moment estimates and $\hat{\mathbf{m}}(t)$ and $\hat{\mathbf{v}}(t)$ are the bias-corrected moment estimates. Here, $\beta_1 = 0.9$ and $\beta_2 = 0.999$ following the original publication;²⁵ $\epsilon = 10^{-7}/\sqrt{1 - \beta_2^t}$ as the default in TensorFlow.

```

init:  $t = 0, \mathbf{m}(0) = 0, \mathbf{v}(0) = 0;$ 
while not converged do
   $t = t + 1;$ 
   $\mathbf{g}(t) = \nabla_{\mathbf{w}} L_2(t);$ 
   $\mathbf{m}(t) = \beta_1 \cdot \mathbf{m}(t - 1) + (1 - \beta_1) \cdot \mathbf{g}(t);$ 
   $\mathbf{v}(t) = \beta_2 \cdot \mathbf{v}(t - 1) + (1 - \beta_2) \cdot \mathbf{g}^2(t);$ 
   $\hat{\mathbf{m}}(t) = \mathbf{m}(t)/(1 - \beta_1^t);$ 
   $\hat{\mathbf{v}}(t) = \mathbf{v}(t)/(1 - \beta_2^t);$ 
   $\mathbf{w}(t) = \mathbf{w}(t - 1) - \eta \cdot \hat{\mathbf{m}}(t)/(\sqrt{\hat{\mathbf{v}}(t)} + \epsilon);$ 
end
return  $\mathbf{w}(t)$ 

```

Algorithm 2: The extended Kalman Filter (EKF) optimizer, where $\boldsymbol{\xi}$ is the error vector at each iteration, \mathbf{J} is the corresponding Jacobian matrix, \mathbf{A} is termed as the scaling matrix, \mathbf{K} is the Kalman gain, \mathbf{P} is the error covariance matrix and the observation-noise covariance matrix \mathbf{R} is set to $\frac{1}{\eta}\mathbf{I}$, with η being the learning rate.²⁰ Following the setting in RuNner¹⁹, the initial $\mathbf{P}(0)$ is set to an identity matrix and the process-noise covariance matrix \mathbf{Q} is set to zero in this work.

```

init:  $t = 0, \mathbf{P}(0) = \mathbf{I};$ 
while not converged do
   $t = t + 1;$ 
   $\mathbf{J}(t) = \nabla_{\mathbf{w}} \boldsymbol{\xi}(t);$ 
   $\mathbf{A}(t) = [\mathbf{J}(t)\mathbf{P}(t - 1)\mathbf{J}^\top(t) + \mathbf{R}(t)]^{-1};$ 
   $\mathbf{K}(t) = \mathbf{P}(t - 1)\mathbf{J}^\top(t)\mathbf{A}(t);$ 
   $\mathbf{P}(t) = [\mathbf{I} - \mathbf{K}(t)\mathbf{J}(t)]\mathbf{P}(t - 1) + \mathbf{Q}(t);$ 
   $\mathbf{w}(t) = \mathbf{w}(t - 1) + \mathbf{K}(t)\boldsymbol{\xi}(t);$ 
end
return  $\mathbf{w}(t)$ 

```

The other optimization algorithm used in this work is EKF, which estimates the internal state of a system given a series of observations over time. In the context of neural network training, it can be interpreted as updating the weights of the neural network according to the gradient of the error with respect to the weights in past samples.²³ The algorithm is summarized in Algo. 2. Note that the notation used here follows Ref. 20, where the learning rate η is controlled by the observation-noise covariance matrix \mathbf{R} . This formulation is more transparent as compared to earlier studies²⁹.

C. Dataset description

Two datasets containing structures, energies and forces of liquid water (and ice phases) were used to train the NNPs in this work. 6324 structures in the BLYP dataset of both liquid phase and ice phases were taken from Ref. 8 and re-computed with the CP2K suite of programs³⁰ and the BLYP functional^{31,32}. The revPBE0-D3 dataset of 1593 structures of liquid water computed with CP2K was directly taken from Ref. 9.

D. Neural Network Potential

1. Network architecture

In this work, the NNPs were constructed using the BPNN architecture,⁶ with the symmetry function taken from Ref. 8. Specifically, 30 symmetry functions for oxygen and 27 for hydrogen were used for the local environment description of atoms. The exact set of symmetry functions used is given in the Supplementary Material (Section A). This local description was fed to an element-specific feed-forward neural network containing 2 hidden layers each comprised of 25 nodes with the tanh activation function and a linear output node to give atomic energy predictions, from which the total energy and force predictions are derived. The weight parameters were initialized using the Nguyen-Widrow method in RuNner,³³ and the Xavier method in PiNN.³⁴

2. Algorithm hyperparameters

The PiNN-Adam models were trained for 5×10^6 steps, with a learning rate η that decays by a factor of 0.994 every 10^4 steps. Notably, the gradient clipping technique was used with the Adam optimizer to alleviate the vanishing and exploding gradients problems.³⁵ Specifically, gradient vectors \mathbf{g} with $\|\mathbf{g}\| > 0.01$ will be scaled by a factor of $0.01/\|\mathbf{g}\|$ during training.

The PiNN-EKF models were trained with a learning rate η for 5×10^5 steps. The RuNner models were trained for 20 epochs (passes of the entire dataset), which corresponds to a total of around 3×10^5 steps. As shown in Algo. 2, the learning rate η of EKF is embedded in the covariance matrix \mathbf{R} and implicitly decays according to the inverse of iteration (see Ref. 36 or Eq. 2 below). η is set to a constant in the PiNN setup; the counterpart of η asymptotically approach unity in the RuNner setup, following the earlier studies.^{19,29}

In both cases, 80% of the dataset were used for training and the rest 20% were left out as a validation set. For each setup, 10 models were trained with different random seeds to split the dataset or initialize the weights of the neural network. Whenever applicable, the standard deviations of the prediction across the models are used as error estimates.

E. Molecular Dynamics Simulation

The molecular dynamics (MD) simulations for all the models were carried out with the ASE code.³⁷ The PiNN code supports calculation with ASE, while the RuNNer code¹⁹ was interfaced to ASE through the LAMMPS³⁸ calculator implemented in ASE. The timestep for all simulations was chosen to be 0.5 fs. For constant particle number, constant pressure and constant temperature (NPT) simulations, the Berendsen barostat and thermostat³⁹ were used to keep the pressure at 1 bar and temperature at 330 or 320 K. For constant particle number, constant volume and constant temperature (NVT) simulations, the Berendsen thermostat was used to keep the temperature at 300 K, and the density was fixed at 1 g/mL. Each MD simulation was run for 100 ps, from which densities or radial distribution functions are computed from the later 50 ps.

III. RESULT AND DISCUSSIONS

A. The extrapolation regime: The case of the BLYP dataset

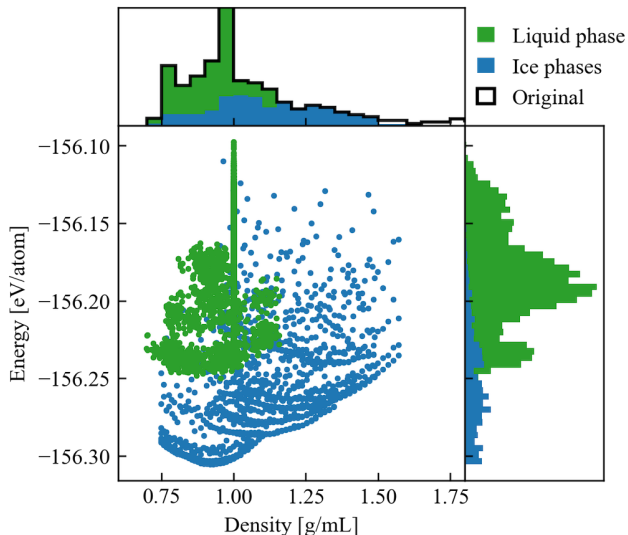


FIG. 2. 2D histogram of the BLYP dataset in terms of the total energy per atom and the bulk density. We excluded a small fraction of the ice-phase structures at very high densities, as compared to the original dataset⁸ (shown as black outline).

The energy-density distribution of the BLYP dataset is shown in Fig. 2. This dataset contains structures from both liquid phase and different ice phases with a peak centering at 1.0 g/mL.⁸ Given the fact that the equilibrium density of the BLYP water at ambient conditions is below 0.8 g/mL,⁸ the isobaric-isothermal density at 1 bar and 330 K will serve as an instructive case study where

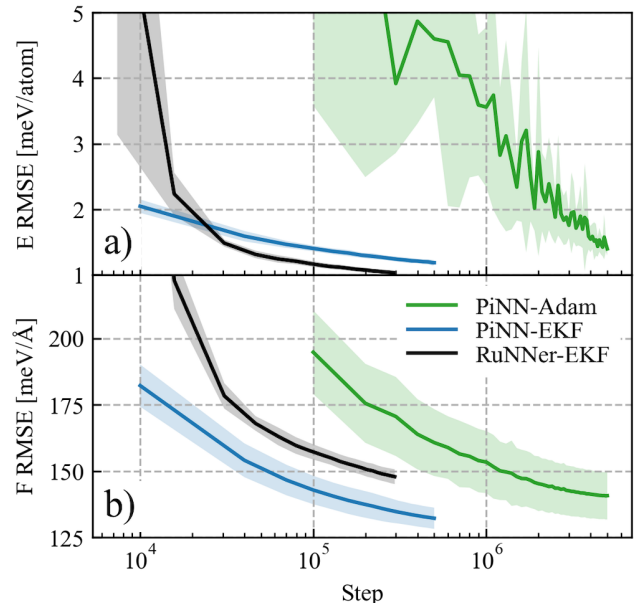


FIG. 3. Training curves of the BLYP dataset for a) energy root mean squared error (RMSE) and b) force RMSE with the Adam and the EKF optimizers.

the NNP is stretched into the extrapolation regime. This motivates us to discuss the result of the BLYP dataset first, where Adam and EKF show qualitative differences. Results shown in this section were generated using the learning rate of 10^{-4} for PiNN-Adam and the learning rate of 10^{-3} for PiNN-EKF, without loss of generality (see Section C in Supplementary Material for details).

Before presenting those results, it is necessary to first discuss the convergence speed of the NNP training. The EKF optimizer is known to converge much faster as compared to Adam (by approximately one order of magnitude in terms of the number of weight updates to achieve the desired accuracy)^{20,40}. This phenomenon is clear in our training of NNPs, as shown in Fig. 3. However, the actual speed-up is compromised due to the higher computational cost of EKF. In practice, the training takes about 2 h for the EKF optimizer and about 5 h for the Adam optimizer on a 28-core computer to achieve similar levels of accuracy in terms of force and energy. It should be noted that the relative speed advantage per iteration increases drastically when the total number of weights grow.

When it comes to the performance of NNPs, one would expect that all the trained potentials with comparable error metrics should yield a consistent water structure at room temperature and experimental density, given the dataset shown in Fig. 2. Indeed, this is borne out, as demonstrated with the O-O radial distribution function in Fig 4a. However, this agreement diverges quickly when it comes to isobaric-isothermal simulations using the same NNPs, as shown in Fig. 4b. This suggests the corresponding densities should also differ from each

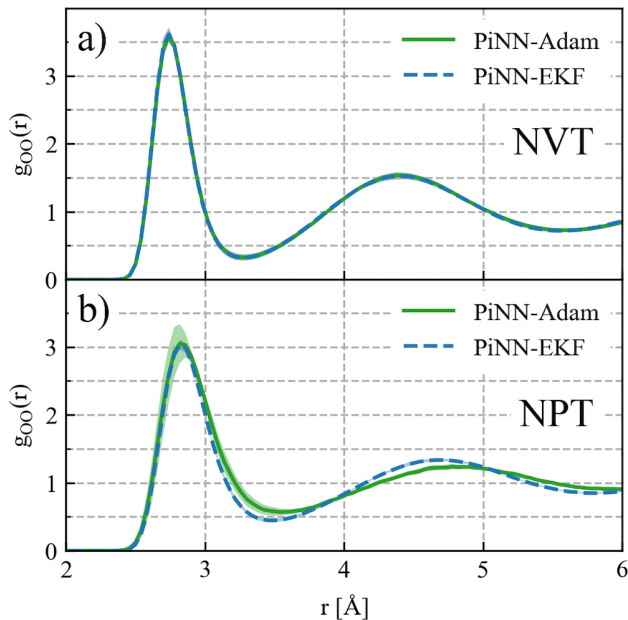


FIG. 4. O-O radial distribution function $g_{OO}(r)$ for a) NVT simulation at 300K, 1g/mL using potentials trained with the Adam and the EKF optimizers; b) NPT simulation at 330K, 1bar using the same potentials. The standard deviations between models are shown as transparent regions, which are small in most cases, except NPT results from PiNN-Adam.

other.

We then proceed to see how well Adam and EKF estimate the isobaric-isothermal density at ambient conditions for the BLYP dataset. As shown in Fig 5, at the pressure of 1 bar and the temperature of 330 K, only 2 out of 10 models trained with Adam manage to predict a stable density, while most of the models trained using EKF lead to an excellent agreement with the previously reported density of around 0.76 g/mL for BLYP water.⁸ In addition, the EKF implementation in PiNN can reproduce the results of RuNNer well for the same dataset.

The qualitative difference between NNPs trained with Adam and EKF seen in Fig. 5 is striking, in light of comparable force and energy errors shown in Fig. 3 and radial distribution functions shown in Fig. 4a. One may argue that the extrapolation is a difficult task for NNPs, because it requires stepping out from their comfort zone. Thus, it is also relevant to consider how the two training algorithms would fare within an interpolation regime. This leads to our second example, the revPBE0-D3 dataset.

B. The interpolation regime: the case of the revPBE0-D3 dataset

In the following experiment, we have used a dataset that was constructed to cover a wide range in the configuration space uniformly,⁹ as seen in the energy-density

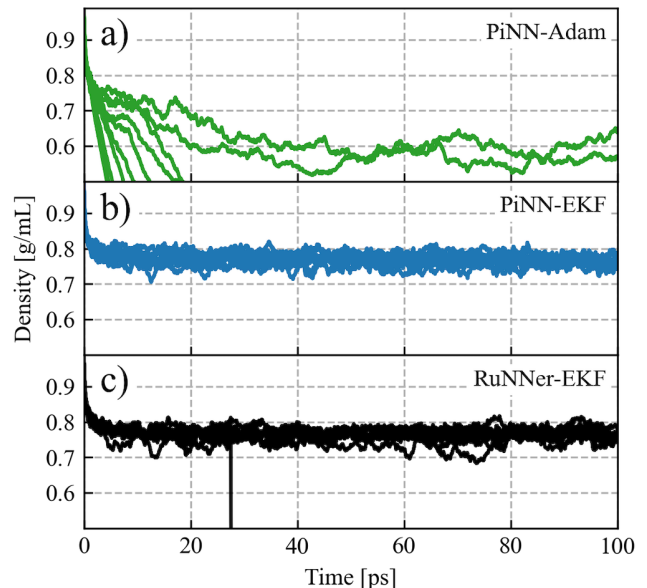


FIG. 5. The density evolution in NPT simulations using potentials trained with a) the Adam, b) and c) the EKF optimizers at 330K and 1bar.

distribution in Fig. 6.

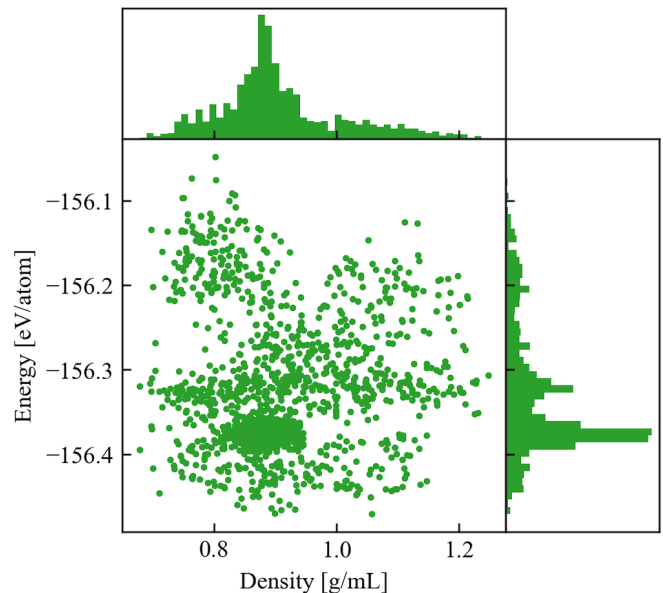


FIG. 6. 2D histogram of the revPBE0-D3 dataset⁹ in terms of the total energy per atom and the bulk density.

With this dataset, both Adam and EKF yield physical densities at the given temperature. All of 10 models trained with Adam, regardless of the learning rate, lead to stable NPT simulations, in stark contrast to the case using BLYP dataset (see Fig. S1 in the Supplementary Material for comparison). However, as shown in Fig. 7,

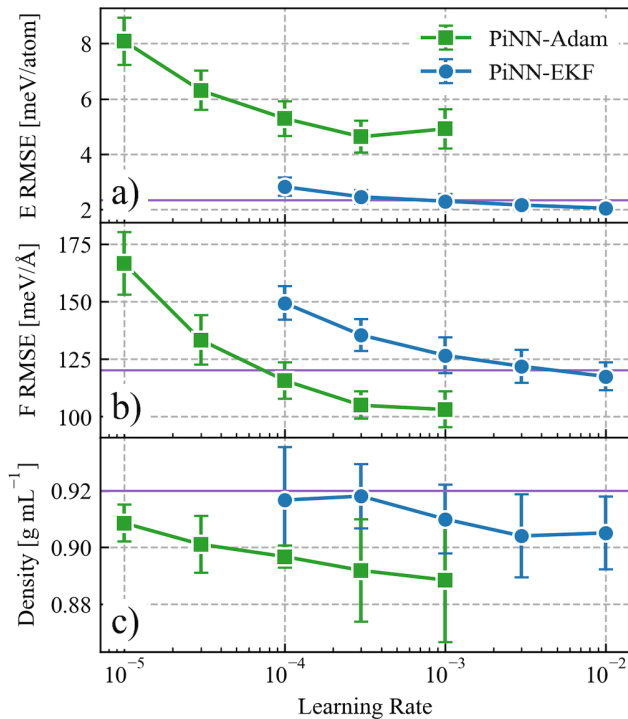


FIG. 7. RMSE and density predictions for NNPs trained with the Adam and the EKF algorithms at different learning rates: a) energy RMSE; b) force RMSE and c) density predictions at 320K, 1bar. Reference values from ref. 9 is shown in purple.

the density prediction strongly depends on the learning rate used to train the model in the case of Adam.

It is tempting to conclude that the models trained with larger learning rates are the better performing ones due to smaller force and energy errors. Similarly to the observation made for the BLYP dataset, the error metrics do not seem to correspond to the actual prediction performance of the trained NNPs. Indeed, we notice that the density does not seem to converge when the error metrics (Fig. 7) have reached lower values. Given that the reference density value for this dataset at 1 bar and 320 K is 0.92 g/ml⁹, this suggests that one has to rethink the common wisdom on performing model selection based on error metrics, such as RMSE.^{41,42}

Regardless of this implication, the present case study demonstrates that the performance of NNPs can be sensitive to the learning rate, in particular for Adam. As a consequence, this can lead to a tangible difference in terms of the density prediction even within the interpolation regime where the dataset already has a good coverage.

C. Differences in models trained using Adam and EKF

In the previous sections, we found that NNPs trained with EKF seem to be less sensitive to the learning rate

and more generalizable. Meanwhile, it is also clear that model selection based on the error metrics of energy and force may not always lead to a sound choice. While unintuitive, the observation is not completely unexpected. The error metrics are typically evaluated on randomly left-out validation sets, which underestimates the generalization error due to their correlation with the training set. Since the training set has to cover sufficient region in the configuration space, it is hard to construct a test set independent of the training set.

Then, the questions are i) can we distinguish “good” and “bad” NNPs by just looking into the weight space (rather than doing the actual MD simulations for the density prediction)? ii) why does EKF do better for training NNPs than Adam?

To answer the first question, we have analysed the models presented in the earlier sections to shed some light on the characteristics of the models trained with Adam and EKF.

One possible measure to distinguish different models is the Euclidean distance of the optimized weights to those in the initialization, which characterizes the implicit regularization effect of stochastic gradient descent.⁴³ Denoting the vector of all weight variables in the neural network as \mathbf{w} , we compared the evolution of the weights distance from initialization $\|\Delta\mathbf{w}\| = \|\mathbf{w} - \mathbf{w}_{\text{init}}\|$, and also the initialization-independent distribution of the weights w_i of the final models for the trained networks.

As shown in Fig 8a, different NNPs trained on the BLYP dataset display similar weights distances from initialization. Moreover, the weight distributions of NNPs trained with Adam and EKF are almost indistinguishable as shown in Fig. 8b. This suggests that the norm-based measure also fails to distinguish models obtained from Adam and EKF. It further hints that using a L_2 norm-based regularization may not improve the performance of NNPs.

Another class of similarity measure is related to the local information geometry of the neural network.⁴⁴ Here, we characterized it with the Fisher information matrix \mathcal{I} :

$$\langle \mathcal{I} \rangle_t = \left\langle (\nabla_{\mathbf{w}} L_1(t))^{\otimes 2} \right\rangle \quad (1)$$

where \otimes^2 denotes the 2nd tensor power of the gradient vector. Here we used L_1 loss instead of L_2 loss to construct the Fisher information matrix for reasons that will be clear later. Fig. 9 shows the distribution of eigenvalues $\lambda_{\mathcal{I}}$ of the Fisher information. For the BLYP dataset, EKF found local minima with much larger eigenvalues as compared to Adam, where the peak of the distribution differs by about one order of magnitude (note the logarithm scale used here). Therefore, the Fisher information is a similarity measure which can effectively distinguish the performance of NNPs.

A similar trend was observed for the revPBE0-D3 dataset. The eigenvalue distribution of NNP trained with Adam and a small learning rate (1E-5) is more

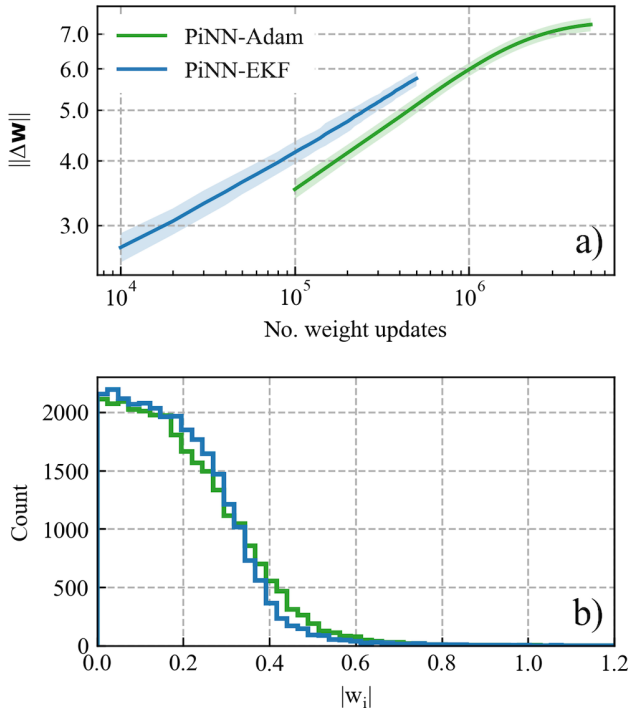


FIG. 8. Weight-based measures for NNPs trained with Adam and EKF for the BLYP dataset: a) the evolution of the Euclidean weight distance from initialization $\|\Delta \mathbf{w}\|$ and b) the initialization-independent distribution of weights w_i .

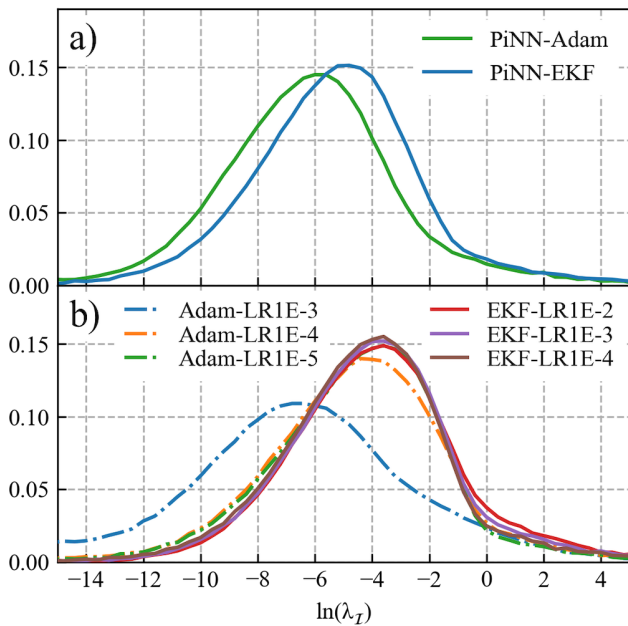


FIG. 9. Distributions of the eigenvalues (λ_I) of the Fisher information matrix: a) with different training algorithms for the BLYP dataset; b) with different training algorithm and learning rates (LR) for the revPBE0-D3 dataset.

close to those trained with EKF. This deviation becomes larger when increasing the learning rate ($1E-4$ and $1E-3$). In contrast, eigenvalue distributions of NNPs trained with EKF are almost identical. These results correlate well with the density prediction from MD simulations as shown in Fig. 7.

The usefulness of the Fisher information for model selection is also linked to the second question posed at the beginning of this section. Despite different motivations, both Adam and EKF can be understood in terms of natural gradient descent (NGD), where the inverse of the Fisher information matrix \mathcal{I} is used as a preconditioner.

In Adam, \mathcal{I} is approximated as a diagonal matrix, with the diagonal terms thereof being the second moment vector $\hat{\mathbf{v}}(t)$. The inverse square root of the diagonal elements are used as a conservative preconditioner.

On the other hand, the connection between EKF and NGD has been shown recently³⁶, where the inverse \mathcal{I} matrix is effectively estimated by the error covariance matrix \mathbf{P} in EKF. In fact, one can show that

$$\mathbf{w}(t) = \mathbf{w}(t-1) - \frac{\eta^2}{2t} \langle \mathcal{I}_1 \rangle_t^{-1} \mathbf{g}(t) \quad (2)$$

when the covariance matrix of observation noise \mathbf{R} in Algo. 2 is chosen to be a scaled identity matrix^{20,36,40}, i.e. $\mathbf{R}(t) = \frac{1}{\eta} \mathbf{I}$.

This means EKF can be viewed as the online estimate of the full Fisher information \mathcal{I} with respect to L_1 loss and the $1/t$ decay of the learning rate. We think such feature leads to a good similarity measure of models using the Fisher information based on Eq. 1 and a superior performance of EKF for training NNPs as demonstrated in two case studies shown in this work.

IV. CONCLUSION AND OUTLOOK

To sum up, we have compared the performance of two optimization algorithms Adam and EKF for training NNPs of liquid water based on BLYP and revPBE0-D3 datasets. It is found that NNPs trained with EKF are more transferable and less sensitive to the choice of the learning rate, as compared to Adam. Further, we show that the Fisher information is a useful similarity measure for the model selection of NNPs when the error metrics and the normal-based measure become ineffective.

Established practice in other neural network applications⁴⁵, using Adam, indicate that practical training performance can be improved if an architecture is reparametrized to promote weights in a common numerical range, without strong correlations. Another future avenue would thus be to preserve the expressive power of existing NNPs, while expressing the weights in such a way that the off-diagonal elements of the resulting Fisher information matrix are minimized. This can be understood in terms of the limitations in the Adam preconditioner strategy.

On the other hand, EKF scales quadratically with the number of trainable parameters in the network, while Adam scales linearly. This makes EKF a less favorable choice when more heavily parameterized models like GCNN^{14–16} are of interest. Necessary approximation to the estimation of \mathcal{I} , such as that based on Kronecker factorization,⁴⁶ is essential to transfer the present observation to those models.

Before closing, it is worth to note that the present issue of training algorithms may be overcome with more data (as shown in Fig. 9 with augmented dataset in our previous work¹⁶), for which a number of active-learning approaches tailored for NNPs have been proposed.^{11,47–50} However, we would argue that a better training algorithm does not only improve the performance of NNPs but also improve the data efficiency in the active-learning.

This work focuses on the practical role of training algorithm in the performance of NNPs, where different approximations to the Fisher information (in Adam and EKF) and the choice of learning rate are factors primarily considered. Nevertheless, as mentioned at the very beginning, other factors, such as loss function and batch schedule, neural network architecture, decay factor and decay steps in training algorithm will bring new dimensions into the discussion. In addition, the examples shown here are based on published dataset of liquid water and the real-application scenario is density prediction. Therefore, the conclusion drawn in this work is yet to be confirmed in more complex systems and other physico-chemical properties, where credible reference values in real-application scenarios can be obtained. Overall, this calls for more systematic investigations to shed light on this topic and the practice of open science to facilitate similar studies in the community. With these efforts, the development of NNPs will become more transparent and reproducible, which in turn will provide reliable insights into interesting chemical physics and physical chemistry problems.

SUPPLEMENTARY MATERIAL

See Supplementary Material for symmetry function parameters, weighting factor in batch schedule and loss function, and learning rate dependency of error metrics and density for the BLYP dataset.

ACKNOWLEDGMENTS

CZ thanks the Swedish Research Council (VR) for a starting grant (No. 2019-05012). We also acknowledge the Swedish National Strategic e-Science program eSENCE for funding. Part of the simulations were performed on the resources provided by the Swedish National Infrastructure for Computing (SNIC) at UPPMAX and NSC.

DATA AVAILABILITY STATEMENT

Datasets used in this work are publicly accessible from DOI: 10.5281/zenodo.2634097 and DOI: 10.24435/materialscloud:2018.0020/v1. The PiNN code is available from <https://github.com/Teoroo-CMC/PiNN> and its EKF implementation will be released in the next version and provided upon request in the interim.

- ¹J. Behler, “Four generations of high-dimensional neural network potentials,” *Chem. Rev.* **121**, 10037–10072 (2021).
- ²V. L. Deringer, A. P. Bartók, N. Bernstein, D. M. Wilkins, M. Ceriotti, and G. Csányi, “Gaussian process regression for materials and molecules,” *Chem. Rev.* **121**, 10073–10141 (2021).
- ³S. Watanabe, W. Li, W. Jeong, D. Lee, K. Shimizu, E. Mimanitani, Y. Ando, and S. Han, “High-dimensional neural network atomic potentials for examining energy materials: some recent simulations,” *J. Phys.: Energy* **3**, 012003 (2020).
- ⁴O. T. Unke, S. Chmiela, H. E. Sauceda, M. Gastegger, I. Poltavsky, K. T. Schütt, A. Tkatchenko, and K.-R. Müller, “Machine learning force fields,” *Chem. Rev.* **121**, 10142–10186 (2021).
- ⁵W. Jia, H. Wang, M. Chen, D. Lu, L. Lin, R. Car, E. Weinan, and L. Zhang, “Pushing the limit of molecular dynamics with ab initio accuracy to 100 million atoms with machine learning,” in *SC20: International Conference for High Performance Computing, Networking, Storage and Analysis* (2020) pp. 1–14.
- ⁶J. Behler and M. Parrinello, “Generalized neural-network representation of high-dimensional potential-energy surfaces,” *Phys. Rev. Lett.* **98**, 146401 (2007).
- ⁷M. Gastegger, J. Behler, and P. Marquetand, “Machine learning molecular dynamics for the simulation of infrared spectra,” *Chem. Sci.* **8**, 6924–6935 (2017).
- ⁸T. Morawietz, A. Singraber, C. Dellago, and J. Behler, “How van der waals interactions determine the unique properties of water,” *Proc. Natl. Acad. Sci. U.S.A.* **113**, 8368–8373 (2016).
- ⁹B. Cheng, E. A. Engel, J. Behler, C. Dellago, and M. Ceriotti, “Ab initio thermodynamics of liquid and solid water,” *Proc. Natl. Acad. Sci. U.S.A.* **116**, 1110–1115 (2019).
- ¹⁰V. Quaranta, M. Hellström, and J. Behler, “Proton-Transfer Mechanisms at the Water-ZnO Interface: The Role of Presolvation,” *J. Phys. Chem. Lett.* **8**, 1476–1483 (2017).
- ¹¹C. Schran, J. Behler, and D. Marx, “Automated fitting of neural network potentials at coupled cluster accuracy: Protonated water clusters as testing ground,” *J. Chem. Theory Comput.* **16**, 88–99 (2019).
- ¹²Y. Shao, M. Hellström, A. Yllö, J. Mindemark, K. Hermansson, J. Behler, and C. Zhang, “Temperature effects on the ionic conductivity in concentrated alkaline electrolyte solutions,” *Phys. Chem. Chem. Phys.* **377**, 1–5 (2020).
- ¹³Y. Lecun, Y. Bengio, and G. Hinton, “Deep learning,” *Nature* **521**, 436–444 (2015).
- ¹⁴K. T. Schütt, H. E. Sauceda, P.-J. Kindermans, A. Tkatchenko, and K.-R. Müller, “SchNet A deep learning architecture for molecules and materials,” *J. Chem. Phys.* **148**, 241722 (2018).
- ¹⁵C. Chen, W. Ye, Y. Zuo, C. Zheng, and S. P. Ong, “Graph Networks as a Universal Machine Learning Framework for Molecules and Crystals,” *Chem. Mater.* **31**, 3564–3572 (2019).
- ¹⁶Y. Shao, M. Hellström, P. D. Mitev, L. Knijff, and C. Zhang, “PiNN: A python library for building atomic neural networks of molecules and materials,” *J. Chem. Inf. Model.* **60**, 1184–1193 (2020).
- ¹⁷M. Gastegger and P. Marquetand, “High-Dimensional Neural Network Potentials for Organic Reactions and an Improved Training Algorithm,” *J. Chem. Theory Comput.* **11**, 2187–2198 (2015).
- ¹⁸N. Artrith and A. Urban, “An implementation of artificial neural-network potentials for atomistic materials simulations: Performance for TiO₂,” *Comput. Mater. Sci.* **114**, 135–150 (2016).

- ¹⁹J. Behler, *RuNNer-A Neural Network Code for High-Dimensional Potential-Energy Surfaces* (2018).
- ²⁰A. Singraber, T. Morawietz, J. Behler, and C. Dellago, "Parallel multistream training of high-dimensional neural network potentials," *J. Chem. Theory Comput.* **15**, 3075–3092 (2019).
- ²¹S.-D. Huang, C. Shang, P.-L. Kang, X.-J. Zhang, and Z.-P. Liu, "LASP: Fast global potential energy surface exploration," *WIREs Comput. Mol. Sci.* **9**, e1415–11 (2019).
- ²²D. C. Liu and J. Nocedal, "On the limited memory BFGS method for large scale optimization," *Math. Program.* **45**, 503–528 (1989).
- ²³S. Singhal and L. Wu, "Training multilayer perceptrons with the extended kalman algorithm," in *Proceedings of the 1st International Conference on Neural Information Processing Systems, NIPS'88* (MIT Press, Cambridge, MA, USA, 1988) p. 133–140.
- ²⁴X. Gao, F. Ramezanghorbani, O. Isayev, J. S. Smith, and A. E. Roitberg, "TorchANI: A free and open source PyTorch-based deep learning implementation of the ANI neural network potentials," *J. Chem. Inf. Model.* **60**, 3408–3415 (2020).
- ²⁵D. P. Kingma and J. Ba, "Adam: A method for stochastic optimization," (2017), arXiv:1412.6980 [cs.LG].
- ²⁶M. Abadi, A. Agarwal, P. Barham, E. Brevdo, Z. Chen, C. Citro, G. S. Corrado, A. Davis, J. Dean, M. Devin, S. Ghemawat, I. Goodfellow, A. Harp, G. Irving, M. Isard, Y. Jia, R. Jozefowicz, L. Kaiser, M. Kudlur, J. Levenberg, D. Mané, R. Monga, S. Moore, D. Murray, C. Olah, M. Schuster, J. Shlens, B. Steiner, I. Sutskever, K. Talwar, P. Tucker, V. Vanhoucke, V. Vasudevan, F. Viégas, O. Vinyals, P. Warden, M. Wattenberg, M. Wicke, Y. Yu, and X. Zheng, "TensorFlow: Large-scale machine learning on heterogeneous systems," (2015), software available from tensorflow.org.
- ²⁷A. Paszke, S. Gross, F. Massa, A. Lerer, J. Bradbury, G. Chanan, T. Killeen, Z. Lin, N. Gimelshein, L. Antiga, A. Desmaison, A. Kopf, E. Yang, Z. DeVito, M. Raison, A. Tejani, S. Chilamkurthy, B. Steiner, L. Fang, J. Bai, and S. Chintala, "Pytorch: An imperative style, high-performance deep learning library," in *Advances in Neural Information Processing Systems 32*, edited by H. Wallach, H. Larochelle, A. Beygelzimer, F. d'Alché Buc, E. Fox, and R. Garnett (Curran Associates, Inc., 2019) pp. 8024–8035.
- ²⁸S. S. Haykin, *Kalman filtering and neural networks* (Wiley, New York; Chichester, 2001).
- ²⁹J. B. Witkoskie and D. J. Doren, "Neural Network Models of Potential Energy Surfaces: Prototypical Examples," *J. Chem. Theory Comput.* **1**, 14–23 (2005).
- ³⁰T. D. Kühne, M. Iannuzzi, M. D. Ben, V. V. Rybkin, P. Seewald, F. Stein, T. Laino, R. Z. Khaliullin, O. Schütt, F. Schiffmann, D. Golze, J. Wilhelm, S. Chulkov, M. H. Bani-Hashemian, V. Weber, U. Borštnik, M. TAILLEFUMIER, A. S. Jakobovits, A. Lazzaro, H. Pabst, T. Müller, R. Schade, M. Guidon, S. Andermatt, N. Holmberg, G. K. Schenter, A. Hehn, A. Bussy, F. Belleflamme, G. Tabacchi, A. Glöb, M. Lass, I. Bethune, C. J. Mundy, C. Plessl, M. Watkins, J. VandeVondele, M. Krack, and J. Hutter, "CP2k: An electronic structure and molecular dynamics software package - quickstep: Efficient and accurate electronic structure calculations," *J. Chem. Phys.* **152**, 194103 (2020).
- ³¹A. D. Becke, "Density-functional exchange-energy approximation with correct asymptotic behavior," *Phys. Rev. A* **38**, 3098 (1988).
- ³²C. Lee, W. Yang, and R. G. Parr, "Development of the Colle-Salvetti correlation-energy formula into a functional of the electron density," *Phys. Rev. B* **37**, 785 (1988).
- ³³D. Nguyen and B. Widrow, "Improving the learning speed of 2-layer neural networks by choosing initial values of the adaptive weights," in *1990 IJCNN International Joint Conference on Neural Networks* (1990) pp. 21–26 vol.3.
- ³⁴X. Glorot and Y. Bengio, "Understanding the difficulty of training deep feedforward neural networks," in *Proceedings of the thirteenth international conference on artificial intelligence and statistics* (2010) pp. 249–256.
- ³⁵R. Pascanu, T. Mikolov, and Y. Bengio, "On the difficulty of training recurrent neural networks," in *Proceedings of the 30th International Conference on Machine Learning*, Proceedings of Machine Learning Research, Vol. 28, edited by S. Dasgupta and D. McAllester (PMLR, Atlanta, Georgia, USA, 2013) pp. 1310–1318.
- ³⁶Y. Ollivier, "Online natural gradient as a Kalman filter," (2018), arXiv:1703.00209 [stat.ML].
- ³⁷A. H. Larsen, J. J. Mortensen, J. Blomqvist, I. E. Castelli, R. Christensen, M. Dulak, J. Friis, M. N. Groves, B. Hammer, C. Hargus, E. D. Hermes, P. C. Jennings, P. B. Jensen, J. Kermode, J. R. Kitchin, E. L. Kolsbjerg, J. Kubal, K. Kaasbjerg, S. Lysgaard, J. B. Maronsson, T. Maxson, T. Olsen, L. Pastewka, A. Peterson, C. Rostgaard, J. Schiøtz, O. Schütt, M. Strange, K. S. Thygesen, T. Vegge, L. Vilhelmsen, M. Walter, Z. Zeng, and K. W. Jacobsen, "The atomic simulation environment—a python library for working with atoms," *J. Phys.: Condens. Matter* **29**, 273002 (2017).
- ³⁸S. Plimpton, "Fast parallel algorithms for short-range molecular dynamics," *J. Comput. Phys.* **117**, 1–19 (1995).
- ³⁹H. J. C. Berendsen, J. P. M. Postma, W. F. van Gunsteren, A. DiNola, and J. R. Haak, "Molecular dynamics with coupling to an external bath," *J. Chem. Phys.* **81**, 3684–3690 (1984).
- ⁴⁰D. Ruck, S. Rogers, M. Kabrisky, P. Maybeck, and M. Oxley, "Comparative analysis of backpropagation and the extended kalman filter for training multilayer perceptrons," *IEEE Transactions on Pattern Analysis and Machine Intelligence* **14**, 686–691 (1992).
- ⁴¹G. Fonseca, I. Poltavsky, V. Vassilev-Galindo, and A. Tkatchenko, "Improving molecular force fields across configurational space by combining supervised and unsupervised machine learning," *J. Chem. Phys.* **154**, 124102 (2021).
- ⁴²D. P. Kovacs, C. van der Oord, J. Kucera, A. Allen, D. Cole, C. Ortner, and G. Csanyi, "Linear atomic cluster expansion force fields for organic molecules: beyond RMSE," *ChemRxiv* (2021), 10.33774/chemrxiv-2021-7qlf5-v3.
- ⁴³V. Nagarajan and J. Z. Kolter, "Generalization in deep networks: The role of distance from initialization," (2019), arXiv:1901.01672 [cs.LG].
- ⁴⁴T. Liang, T. Poggio, A. Rakhlin, and J. Stokes, "Fisher-Rao metric, geometry, and complexity of neural networks," (2019), arXiv:1711.01530 [cs.LG].
- ⁴⁵S. Ioffe and C. Szegedy, "Batch normalization: Accelerating deep network training by reducing internal covariate shift," in *Proceedings of the 32nd International Conference on Machine Learning*, Proceedings of Machine Learning Research, Vol. 37, edited by F. Bach and D. Blei (PMLR, Lille, France, 2015) pp. 448–456.
- ⁴⁶J. Martens and R. Grosse, "Optimizing neural networks with Kronecker-factored approximate curvature," (2015), arXiv:1503.05671 [cs.LG].
- ⁴⁷N. Artrith and J. Behler, "High-dimensional neural network potentials for metal surfaces: A prototype study for copper," *Phys. Rev. B* **85**, 045439 (2012).
- ⁴⁸J. S. Smith, B. Nebgen, N. Lubbers, O. Isayev, and A. E. Roitberg, "Less is more: Sampling chemical space with active learning," *J. Chem. Phys.* **148**, 241733 (2018).
- ⁴⁹Y. Zhang, H. Wang, W. Chen, J. Zeng, L. Zhang, H. Wang, and W. E, "DP-GEN: A concurrent learning platform for the generation of reliable deep learning based potential energy models," *Comput. Phys. Commun.* **253**, 107206 (2020).
- ⁵⁰C. Schran, F. L. Thiemann, P. Rowe, E. A. Müller, O. Marsalek, and A. Michaelides, "Machine learning potentials for complex aqueous systems made simple," *Proc. Natl. Acad. Sci. U.S.A.* **118**, e2110077118 (2021).

Supplementary Material

Training Algorithm Matters for the Performance of Neural Network Potential: A Case Study of Adam and the Kalman Filter Optimizers

Yunqi Shao,[†] Florian M. Dietrich,[†] Carl Nettelblad,[‡] and Chao Zhang^{*,†}

[†]*Department of Chemistry-Ångström Laboratory, Uppsala University, Lägerhyddsvägen 1,
BOX 538, 75121, Uppsala, Sweden*

[‡]*Department of Information Technology, Uppsala University, Lägerhyddsvägen 2, BOX
337, 75105, Uppsala, Sweden*

E-mail: chao.zhang@kemi.uu.se

A. Symmetry Function Parameters

In this work, atomistic descriptions are given with the G^2 and G^3 symmetry functions:¹

$$G_i^2 = \sum_j e^{-\eta(r_{ij}-r_s)^2} \cdot f_c(r_{ij}) \tag{1}$$

$$G_i^3 = 2^{1-\zeta} \sum_{j \neq i} \sum_{k \neq i, j} [(1 + \lambda \cdot \cos \theta_{ijk})^\zeta \cdot e^{-\eta(r_{ij}^2+r_{ik}^2+r_{jk}^2)} \cdot f_c(r_{ij}) \cdot f_c(r_{ik}) \cdot f_c(r_{jk})] \tag{2}$$

$$f_c(r_{ij}) = \tanh^3(1 - r_{ij}/r_c) \tag{3}$$

where $f_c(r)$ is the cutoff function; $r_c = 12$ Bohr for all symmetry functions; and η , r_s and λ are parameters that specify the shape of the symmetry functions. The parameters for the G^2 and G^3 symmetry functions used in this work is listed in Table. S1 and S2. The symmetry functions are then scaled to the interval $[-1, 1]$ according to their range in the training set, by applying:

$$G_i^{\text{scaled}} = \frac{2(G_i - G_{i,\min})}{G_{i,\max} - G_{i,\min}} - 1 \tag{4}$$

Table S1: Definition of G^2 symmetry in the description, for each combination of element pair and r_s , a set of symmetry functions is used whose η parameters are enumerated.

Element i	Element j	r_s [Bohr]	η [Bohr ⁻²]
H	H	0.0	0.001, 0.01, 0.03, 0.06
H	H	1.9	0.15, 0.30, 0.60, 1.50
H	O	0.0	0.001, 0.01, 0.03, 0.06
H	O	0.9	0.15, 0.30, 0.60, 1.50
O	H	0.0	0.001, 0.01, 0.03, 0.06
O	H	0.9	0.15, 0.30, 0.60, 1.50
O	O	0.0	0.001, 0.01, 0.03, 0.06
O	O	4.0	0.15, 0.30, 0.60, 1.50

Table S2: Definition of G^3 symmetry in the description, for each combination of element triplet and λ , a set of symmetry functions is used whose η and ζ parameters are enumerated.

Element i	Element j	Element k	λ	ζ	η [Bohr ⁻²]
H	H	O	1.0	4.0, 1.0, 1.0, 1.0	0.01, 0.03, 0.07, 0.20
H	H	O	-1.0	4.0, 1.0, 1.0	0.01, 0.03, 0.07
H	O	O	1.0	4.0, 1.0	0.001, 0.03
H	O	O	-1.0	4.0, 1.0	0.001, 0.03
O	H	H	1.0	4.0, 1.0, 1.0	0.01, 0.03, 0.07
O	H	H	-1.0	4.0, 1.0, 1.0	0.01, 0.03, 0.07
O	H	O	1.0	4.0, 1.0	0.001, 0.03
O	H	O	-1.0	4.0, 1.0	0.001, 0.03
O	H	H	1.0	4.0, 1.0	0.001, 0.03
O	H	H	-1.0	4.0, 1.0	0.001, 0.03

B. Weighting Factor in Batch Schedule and Loss Function

The difference in the scheduling of labels means the frequency and weighing factor of weight updates with energy and force labels in RuNNer and PiNN are different. However, the error vector and the loss function used are consistent between PiNN-Adam and PiNN-EKF. The approximated number of updates for each type of label per epoch, and the weighting-factor ratio for energy and force losses for both setups are listed in Table. S3.

Table S3: Estimated number of steps used per epoch and weighing factor for energy (E) and force (F) labels in RuNNer and PiNN batch schedules. This estimation is obtained according to the statistics gathered when training on the BLYP dataset. The weighting factors used in the loss function are given in atomic units. Note that in the RuNNer batch schedule, the update refers to that based on a single label, which are subsequently applied in groups of 10 labels. The labels are filtered according to relative error in the RuNNer scheduling, therefore the number of updates are given in as ranges. The relative weighing factor c_E/c_F in the RuNNer setup is automatically adjusted according to the number of force and energy labels in each structure. Here, typical values (corresponding to structures with 16 water molecules) are given.

	E updates	F updates	c_E/c_F [a.u.]
PiNN	~2500	~2500	0.28
RuNNer	~900–3000	~6000–14000	3.69–14.75

C. Learning rate dependency of error metrics and density for the BLYP dataset

The effect of learning rate on the error metrics and density prediction for the BLYP dataset is shown in Fig. S1. In the Main Text, the learning rate for Adam is set to 10^{-4} to represent the best hyperparameter determined by the error metrics; the learning rate for EKF is set to 10^{-3} .

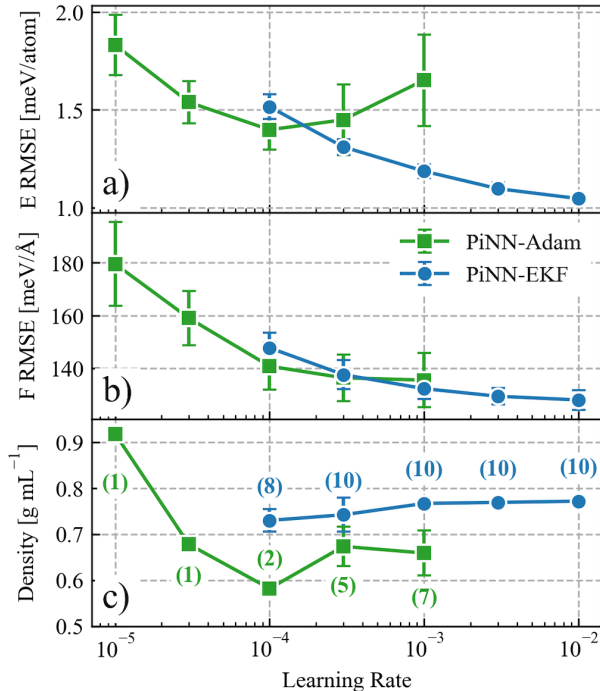


Figure S1: RMSE and density predictions for NNPs trained with the Adam and the EKF algorithms at different learning rates: a) energy RMSE; b) force RMSE and c) density predictions at 330K, 1bar. The error bars are estimated using the standard deviation between models trained with the same setup whenever possible. The number of models (out of 10 instances) that predict stable densities is annotated in the parentheses in panel c.

References

- (1) Behler, J. RuNNer-A Neural Network Code for High-Dimensional Potential-Energy Surfaces. 2018.